Tunable long-wavelength interdiffused quantum-well photodetector

Alex S. W. Lee and E. Herbert Li

Department of Electrical and Electronic Engineering, University of Hong Kong
Pokfulam Road, Hong Kong

Abstract

A wide tunable long-wavelength AlGaAs/GaAs quantum well intersubband photodetector is theoretically analyzed for various stages of interdiffusion. Both the absorption strength and responsivity are enhanced for certain extents of interdiffusion and the peak detection wavelength can be red shifted continuously over a large tunable range. The dark current increases with interdiffusion but is acceptable for smaller diffusion extent.

Keywords: Photodetector, Intersubband transition, Interdiffusion, quantum well, AlGaAs/GaAs, Dark Current, Responsivity

Introduction

In recent years, devices based on intersubband absorption have been the subject of numerous studies and its potential applications for infrared (IR) detection,[1] moduclation,[2] and no-linear devices[3] have been investigated. Owing to the mature of III-V materials and processing technologies, there has been much progress in quantum well infrared photodetectors (QWIPs).[4-7] The principal operation parameters of QW, such as quantized energy levels, are determined by the QW confinement profile and which depend on the dimension and alloy composition of the well and barrier. However, the designed QW structure may not always turn out to be expected after growth due to the inhomogeneities in well width, the non-constant growth rate of the GaAs and AlAs, or the failure in precisely controlling the evaporation rate of Ga and Al during growth. These may lead to a lower yield rate since the electronic and optical properties of a QW requires a fairly precise accuracy. On the other hand, interdiffusion provides a means to offer the flexibility to modify the properties of the material after growth. It has been demonstrated that the intersubband transition energy in a partially diffused quantum well (DFQW) can be red shifted[8] and postgrowth tuning of the peak detection wavelength can be achieved in QW IR-detectors using rapid thermal annealing.[9] In this letter, we present the advantage of using the DFQW to modify the intersubband optical spectrum, such as absorption peak wavelength and spectral width. We will also demonstrate enhanced performance of the DFQW photodetector in absorption and responsivity with a wide tunable detection wavelength from 7 to 38.4 μm. The red shift of the peak can be related to the variation of DFQW profile during interdiffusion.

0-8194-2298-3/96/$6.00

Model

DFQW is formed by the interdiffusion of Al and Ga atoms across the well and barrier interface at a certain time and high enough temperature. The extent of interdiffusion is characterized by the diffusion length $L_d=(Dt)^{1/2}$, where D is diffusion coefficient and t is diffusion time. The as-grown square QW is defined by $L_d = 0$ and a small value of L_d corresponds to a slightly interdiffused QW, while a large value of L_d corresponds to an extensively interdiffused QW. The diffused Al composition profile, w(z), across the QW structure is given by[10]

$$w = w_0 \left\{1 - \frac{1}{2} - \left[\mathrm{erf}\left[\frac{L_z + 2z}{4L_d}\right] + \mathrm{erf}\left[\frac{L_z - 2z}{4L_d}\right]\right]\right\} \tag{1}$$

where w_o is the as-grown Al mole fraction in the barrier, L_z is the grown axis (QW centered at z=0), and erf denotes the error function, L_d is the diffusion length. The DFQW confinement profile for the conduction band, $U_c(z)$ modeled by error function , is defined by: $U_c(z) = Q_c\,[E_g(z)-E_g(z=0)]$, where $Q_c=0.65$ is the band offset ratio and $E_g(w) = 1.424+1.594w+w(1-w)(0.127-1.31w)$ is the bulk bandgap at room temperature. The other material parameters are adapted from reference 9. Using the Ben-Daniel and Duke model with a z-position dependent effective mass on the interdiffused composition profile, the energies of these states (E_{c1}, E_{c2} , ...) can be solved by the Schrodinger equation using a finite difference method .[10]

There are two sets of DFQW structures in this study. Sample 1 consists of 50 periods 40 Å wide as-grown QW, alternating with 500 Å $Al_{0.3}Ga_{0.7}As$ barrier layers. It is designed to have only one bound state in the well. While sample 2 consists of 50 periods 55 Å well width and 500 Å $Al_{0.24}Ga_{0.76}As$ barrier layers. It contains two bound states in the well. Both QW structures are n-type doped with $1x10^{18}$ cm^{-3} Si and the material are interdiffused with different diffusion extents. The model of intersubband-band absorption in the QWs is based on the one-electron density matrix formulation[11] with P-polarized incident photon, i.e. the electric field vector $\hat{E}$ of the incident optical wave is oriented along the QW confinement direction (z axis) and takes into account the intrasubband relaxation. The absorption coefficient, α, is given by

$$\alpha = \frac{\omega}{c_0 n_r \varepsilon_0} |M_{fi}|^2 \left(\frac{m^* k_B T}{L_z \pi \hbar^2}\right) \times \ln\left(\frac{1+\exp\left(\frac{E_F - E_i}{k_B T}\right)}{1+\exp\left(\frac{E_F - E_f}{k_B T}\right)}\right) \times \frac{\frac{\hbar}{\tau_{if}}}{\left(E_f - E_i - \hbar\omega\right)^2 + \left(\frac{\hbar}{\tau_{if}}\right)^2} \quad , \tag{2}$$

where ω is the photon frequency, μ is the permeability of the material, c_o is the light velocity, L_z is the well width, m^* is the effective mass of electron, ε_o is the permitivity in vacuum, $|M_{if}|^2$ is the dipole matrix elements, $n_r=3.2$ is the is the refractive index and $\tau_{if}=90$ fs is the intrasubband relaxation time.[12]

The responsivity, $\Re$, is defined as the ratio between the output signal and the radiant input and is given by [5]

$$\Re(\upsilon)= \frac{e}{h\nu} g\eta(\upsilon)P_e \tag{3}$$

where

$$\eta(\nu) = \frac{1}{2}(1 - e^{-2\alpha(\nu)L_p}) \tag{4}$$

is the quantum efficiency and the factor 2 accounts for the increased absorption due to the reflection off the top metallic contact,[4] α is the absorption coefficient, g= L/*l* is the optical gain where L is the hot-electron mean free path, and *l* is the device length and $P_e=(1 + \tau_e/\tau_r)^{-1}$ is the tunneling escape probability[5] where τ_e is the escape time from the vicinity of the well and τ_r is the recapture time. The factors g=0.5 and P_e= 0.8 are taken for bound-to-continuum transition and g=0.3 and P_e= 0.5 for bound-to-bound transition for simplicity of calculation.

The dark current is calculated by [1]

$$I_D(v)=An_t(v)ev_d(v) \tag{5}$$

where A is the detector area, e is the electronic charge, $v_d(v)$ is the conduction band drift velocity and is given by

$$v_d = \frac{\mu V}{L_p}\left[1+(\frac{\mu V}{v_s L_p})^2\right]^{-1/2} \tag{6}$$

where *F* is the average field, v_s= 5x10^{-6} is the saturation drift velocity and μ= 1200 cm^2/Vs is the mobility. n_t is the carrier density laying above the barrier conduction band edge and is given by

$$n_t = \frac{1}{L_p}\int_{Eo}^{\infty} T(E,V) f(E)\rho(E)dE \tag{7}$$

where L_p is the DFQW period, V is the potential drop across a period, E is the total energy, E_o is the ground state energy, $f(E) = [1 + \exp(E - E_o - E_F)/kT]^{-1}$ is the Fermi factor, E_F is the two-dimensional Fermi level, $\rho(E)$ is the two dimensional density of state in the QW, and T(E,V) is the bias-dependent tunneling probability through a single barrier and was calculated using the WKB method. In our calculation, T(E,V)= 1 is taken for $E > V_o$, where V_o is the barrier height and for different energy range,

$$T(E,V) = \exp[(-4L_p/3ev)(2m^*/\hbar^2)^{1/2}(V_o - E)^{3/2}] \tag{8}$$

for $V_0 - eV < E < V_o$ and

$$T(E,V) = \exp\{(-4L_p/3ev)(2m^*/\hbar^2)^{1/2}[(V_o - E)^{3/2} - (V_o - E - eV)^{3/2}]\} \tag{9}$$

for $E_o < E < V_o - eV$

Results and Discussion

Fig. 1 shows the room temperature intersubband absorption peak, α_p, for sample 1 and Fig. 2 for sample 2, with several L_d ranging from 0 to 40 Å. It can be seen that the absorption peak increases for both samples, from α_p= 369 cm^{-1} (L_d = 0, i.e. an as-grown square QW where the first excited state is in the continuum) to α_p= 4297 cm^{-1} (L_d= 20 Å) for sample 1 and from α_p= 4653 cm^{-1} (L_d= 0) to α_p= 5005 cm^{-1} (L_d=15 Å) for sample 2, and then followed by a gradual monotonic decrease. The large enhancement in absorption strength is due to the fact that as interdiffusion proceeds, the intermixing of Al and Ga will result in a graded well shape where the ground state energy, first excited state energy, and the barrier height will be modified as shown in Fig. 3 and Fig. 4. For sample 1 at L_d= 20 Å, the first excited state is localized and bound in the DFQW at about 11 meV below the top of the well, whose envelope wave function strongly overlaps with the ground state one and results in a larger oscillator strength. The same occurs to sample 2 at L_d=15 Å where the first excited state is about 12 meV below the top of the well even though the sample has been designed to have two bound states in the well, which may give a larger oscillator strength. Our result shows that the largest absorption strength may occur only when the first excited state has been modified by interdiffusion to the right position. This is consistent with the theory that the largest oscillator strength occurs when the first excited state is close to the top of the well[13,14] which leads to an improved absorption strength. It is interesting to note that even though the ground state energy increases with L_d at the initial stage of interdiffusion, the intersubband transition energy shows no abrupt change but a monotonic red-shifts to longer wavelength and almost saturated at L_d= 40 Å, as shown in the insert of Fig. 3 and 4. This phenomenon agrees well with the experimental data[7] although derails of the ground stated variation has not been shown there. Note also that the absorption peak of sample 2 decreases at L_d= 5 Å. This is because at the initial stage of interdiffusion, the effective well width at the top of the DFQW increases so that the first excited wave function spreads broader in the well, which gives a smaller dipole matrix element and, hence, a smaller absorption strength. For a larger interdiffusion extent (L_d > 25 Å) , the DFQW begins to `flatten' out with a wider effective well width and a lower barrier height, where the wave function extends far into the barrier. This reduces the quantum confinement effect and consequently a high probability for charges transfer out of the well, and which leads to a reduced absorption strength, as shown in Fig. 1 and 2.

Fig. 5 shows the calculated responsivity spectra of sample 1 for a 10 kV/cm electric field at 77 K and different L_d. It can be seen that the responsivity spectrum increases in amplitude and narrows in linewidth as Ld increases to 20 Å. As interdiffusion proceeds further, it reduces in amplitude while the linewidth becomes broader again. The peak responsivity red-shifted through out the range of interdiffusion considered here. Note that the response spectra remain broader for L_d smaller than 10 Å. This is due to the bound-to-continuum transition where the first excited state remains above or at almost the same height as the barrier, and its wave function spreads over the continuum. For L_d larger than 10 Å, the first excited state becomes more localized and bound within the DFQW. The transition is now bound-to-bound which leads to a larger oscillator strength and narrower linewidth as shown in Fig. 5. The broadening of the spectra at even larger L_d is due to the flattening of the well shape, thus gradually losing its quantum confinement. With an applied field, the barrier height will be further reduced and this makes the DFQW even more flattened and bulk-like in nature, and which leads to a smaller oscillator strength. The lowering of the barrier height reduces the tunneling time of the photoexcited electron out f

the well which contributes to the broadening effect.[5] Since the time constant in our model is fixed, we exclude this mechanism.

Dark current is analyzed here for sample 1 for different L_d at T= 77 K, as shown in Fig. 6. The dark current is increased by about 8 orders as L_d increases from 0 to 40 Å. However, the rate of increase of dark current decreases with increasing L_d. This is not surprising because the barrier height decreases with increasing L_d, as shown in Fig. 3. Since tunneling through the top of the barrier is the major contribution to the dark current, the lowering of the barrier will assist the non-photoexcited electron to tunnel out of the well. This agrees well with experimental report[6] by varying both the well and barrier thickness of square QWs. Note that the dark current of L_d= 0 and 5 Å does not overlap but differs by an order even though they are of the same barrier height. This is owing to the increase of ground state energy which is due to a narrower effective well width of the DFQW profile during the initial stages of interdiffusion, as shown in Fig. 3. The dark current increase linearly for bias > 1 V. Since the bottom of the square well will be changed gradually into a graded shape by interdiffusion, this will add to the barrier effectively an additional thickness to impede the tunneling of electrons so that the dark current will increase with a smaller gradient.

Conclusion

In summary, we have reported a wide tuning range and an enhanced performance DFQW photodetector at various L_d. Absorption strength as well as responsivity can be enhanced and the detection wavelength can be tuned by modifying the energy levels of the QW through interdiffusion. Dark current increases by a few order with interdiffusion due to the lowering of the barrier height. But for L_d < 15 Å (sample 1) and small bias, the dark current is at an acceptable level for infrared detection applications. Optimizing the design of the DFQW will be able to reduce the dark current at larger L_d.

Acknowledgment

The author would like to thank the HKU-CRCG and RGC-Earmarked Research Grant for financial support.

Reference

1. B. F. Levine, C. G. Bethea, G. Hasnain, V. O. Shen, E. Pelve, R. R. Abbott, and S. J. Hsieh, Appl. Phys. Lett. **56**, 851 (1990)
2. R. P. G. Karunasiri, Y. J. Mii, and K. L. Wang, IEEE Electron. Device. Lett. **11**, 227, (1990)
3. E. Rosencher, P. Bois, J. Nagle, E. Costard, and S. Delaitre, Appl. Phys. Lett. **55**, 1597, (1989)
4. B. F. Levine, K. K. Choi, C. G. Bethea, J. Walker, and R. J. Malik, Appl. Phys. Lett. **51**, 934 (1987)
5. B. F. Levine, C. G. Bethea, K. K. Choi, , J. Walker, and R. J. Malik, Appl. Phys. Lett. **53**, 231 (1988)
6. H. C. Liu, A. G. Steel, M. Buchanan, and Z. R. Wasilewski, pg 57, Intersubband Transitions in Quantum Wells, edited by E. Rosencher, B. Vinter, and B. Levine, Sept, (Plenum, New York, 1992)
7. B. F. Levine, A. Zussman, S. D. Gunapala, M. T. Asom, J. M. Kuo, and W. S. Hobson, J. Appl. Phys. **72**, 4429 (1992)
8. J. D. Ralston, M. Ramsteiner, B. Dischler, G. Brandt, P. Koidl, and D. J. As, J. Appl. Phys. **70**, 2195 (1991)
9. A. G. Steele, M. Buchanan, H. C. Liu, and Z. R. Wasilewski., J. Appl. Phys. **75**, 8234 (1994)
10. E. H. Li, B. L. Weiss, and K. S. Chan, Phys. Rev. B. **46**, 15180 (1992)
11. D. Ahn and Chuang, S. L. IEEE J. Quantum Electron. **23**, 2196 (1987)
12. R. Ferreira and G. Bastard, Phys. Rev. B. **40**, 1074 (1989)
13. D. D. Coon and R. P. G. Karunasiri, Appl. Phys. Lett. **45**, 649 (1984)
14. A. G. Steele, H. C. Liu, M. Buchanan, and Z. R. Wasilewski, Appl. Phys. Lett. **59**, 3625 (1991)

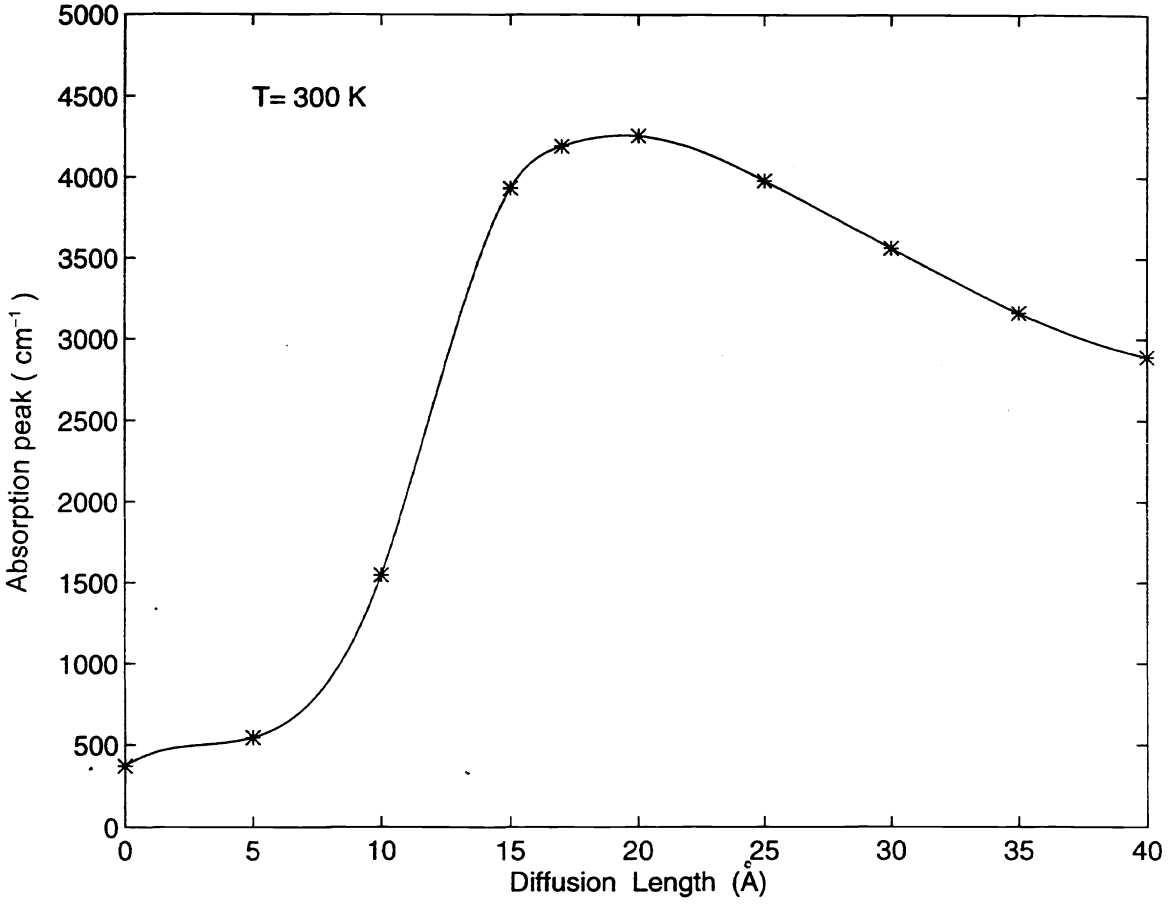

Fig. 1. Sample 1 room temperature absorption peak for L_d=0~40 Å of $Al_xGa_{1-x}As$/GaAs DFQW (x= 0.3, well width = 40 Å).

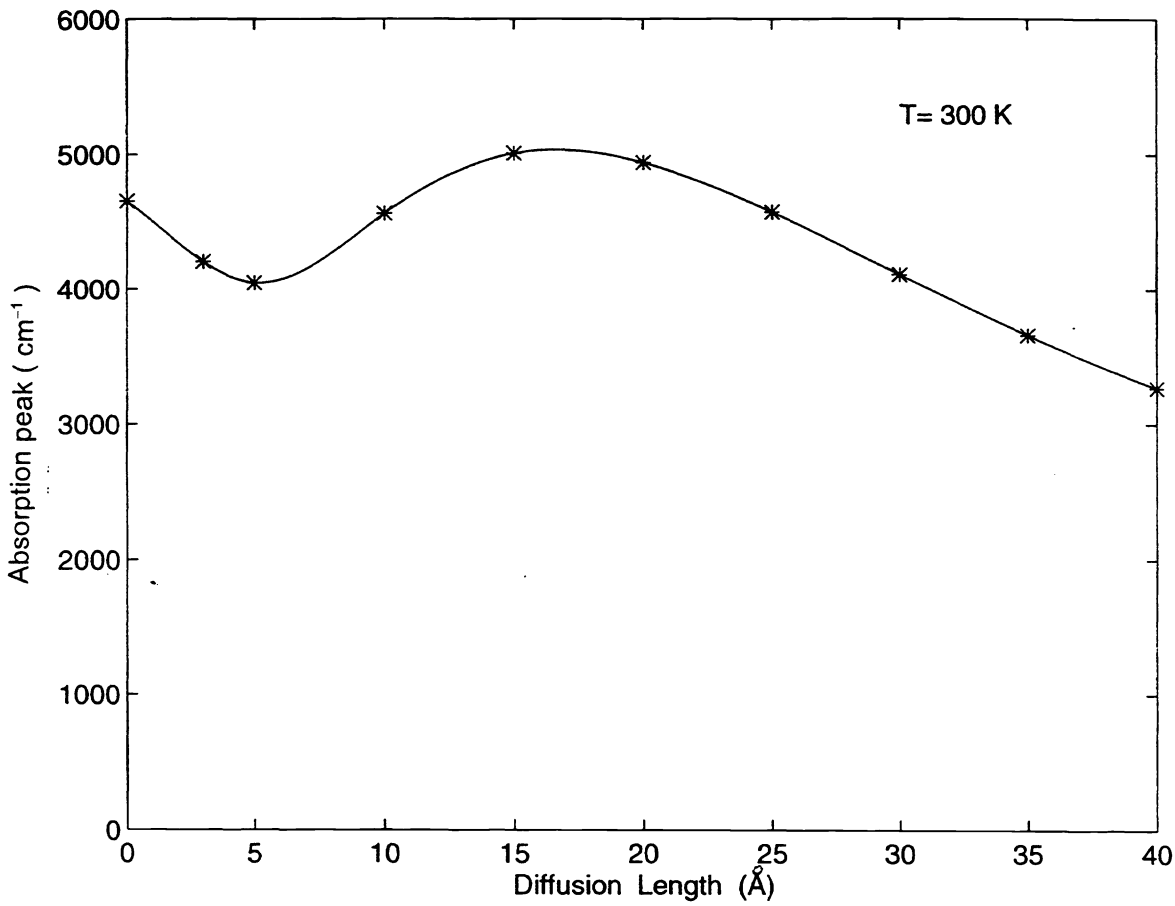

Fig. 2. Sample 2 room temperature absorption peak for L_d=0~40 Å of $Al_xGa_{1-x}As$/GaAs DFQW (x= 0.24, well width = 55 Å).

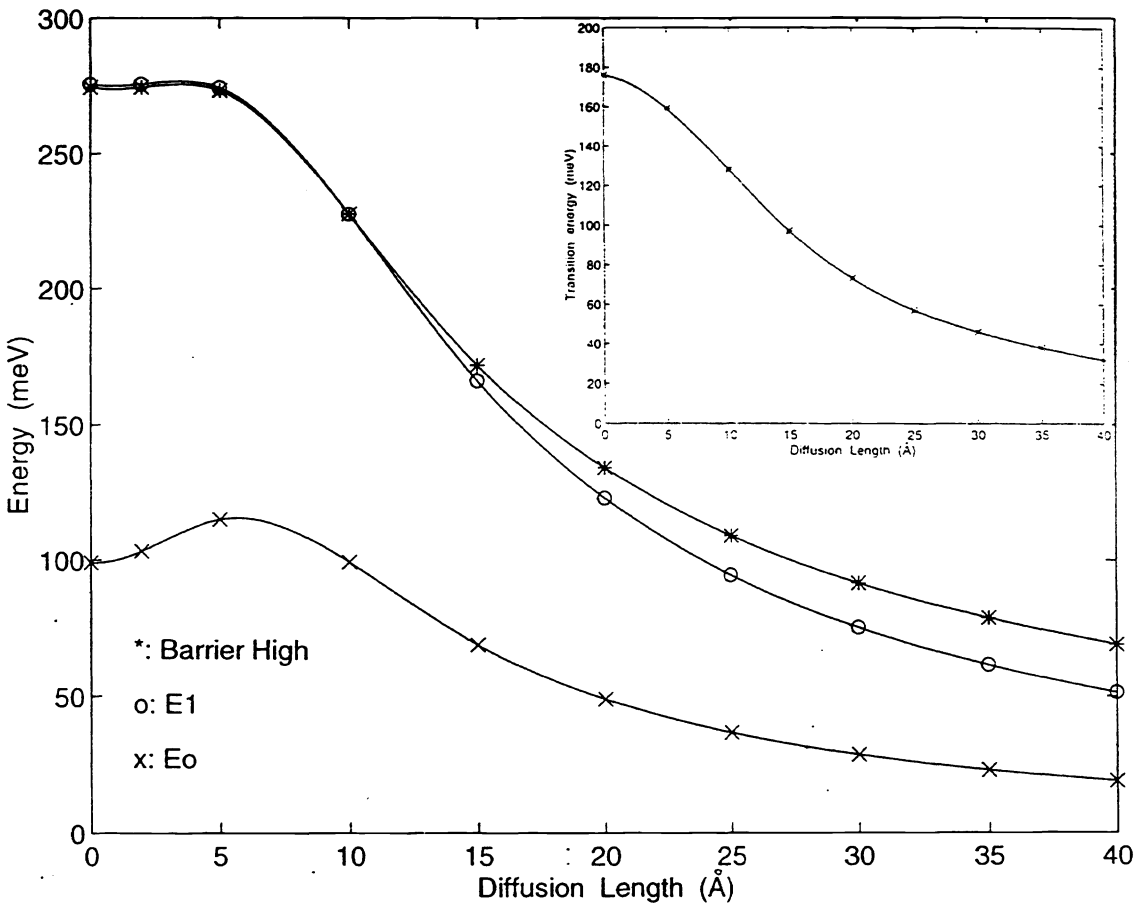

Fig. 3. Variation of energy levels of sample 1 for L_d= 0~40 Å. Insert is the transition energy for different L_d.

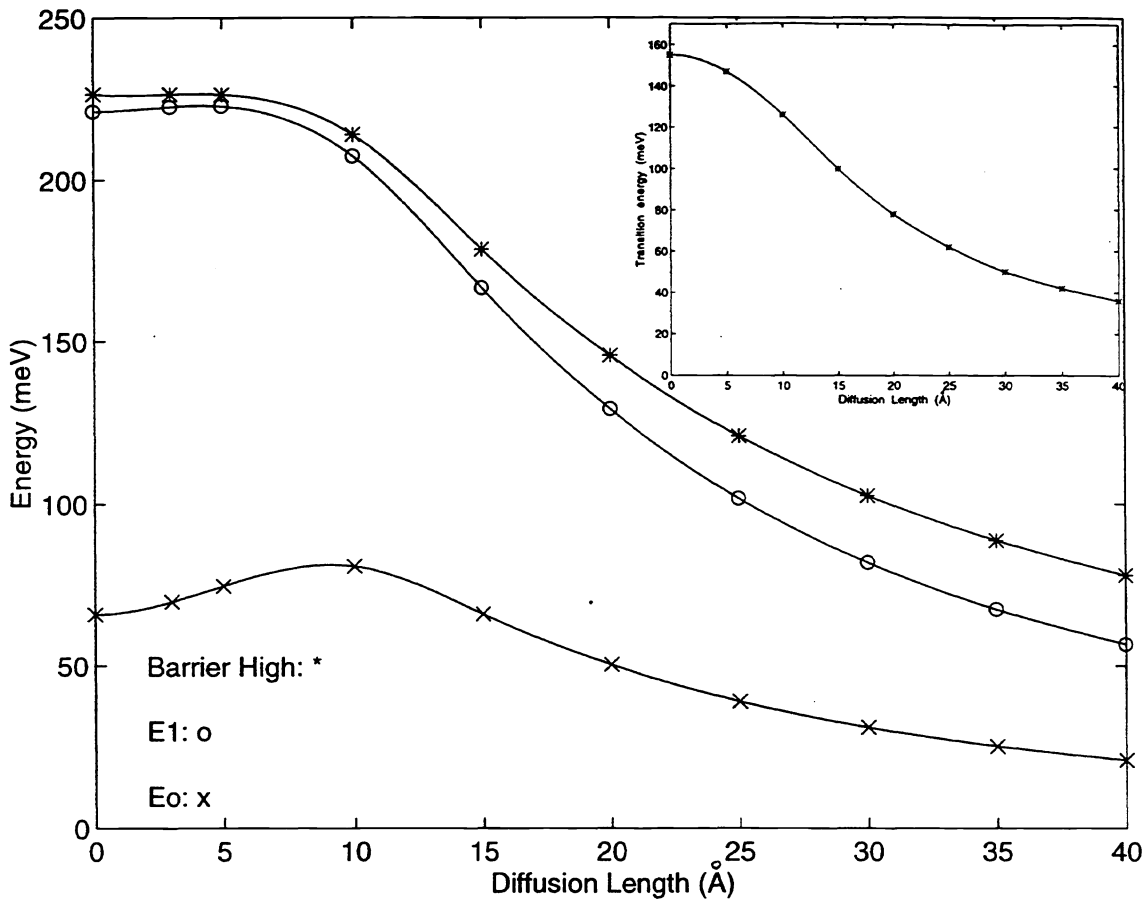

Fig. 4. Variation of energy levels of sample 2 for L_d= 0~40 Å.
Insert is the transition energy for different L_d.

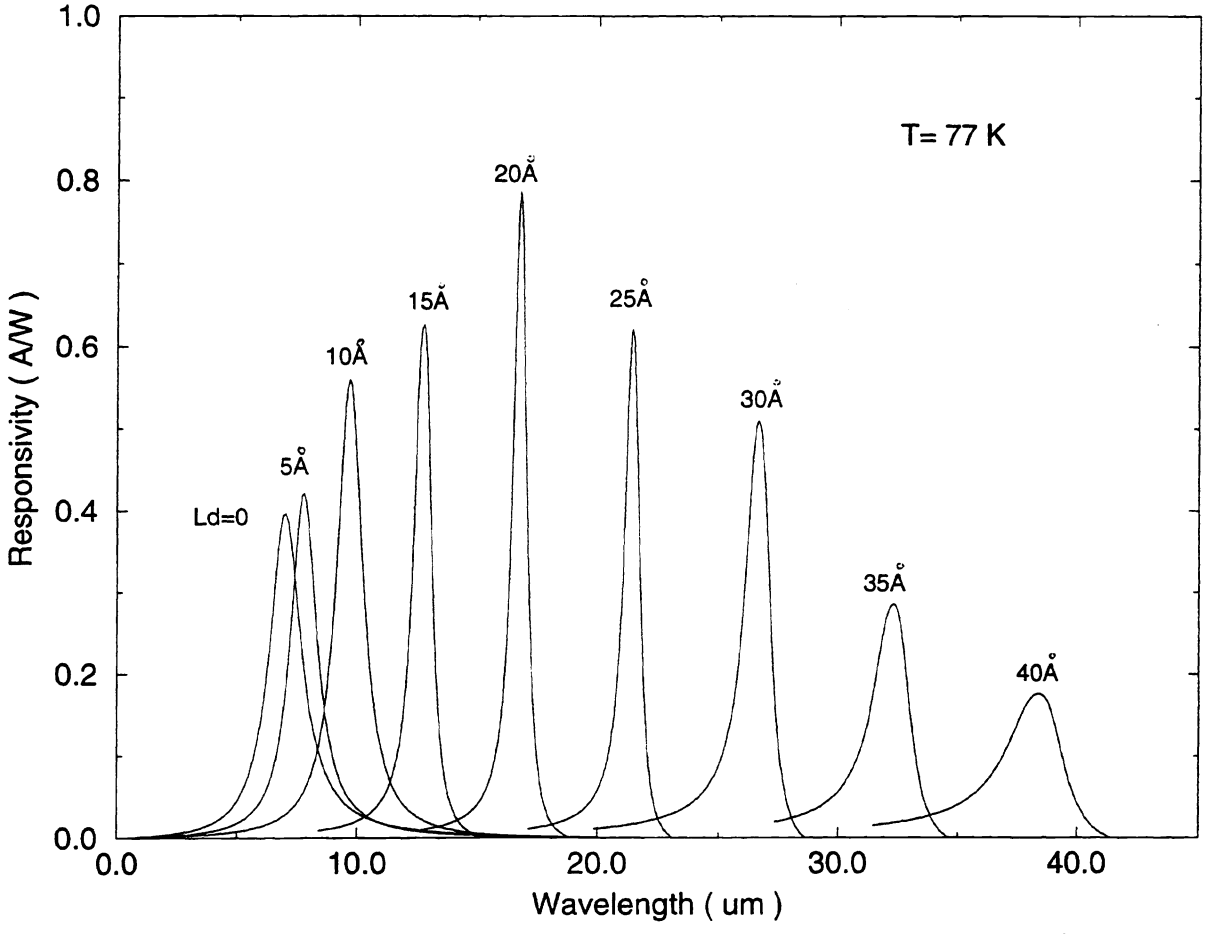

Fig. 5. Responsivity spectra of sample 1 at T= 77 K for L_d= 0~40 Å.

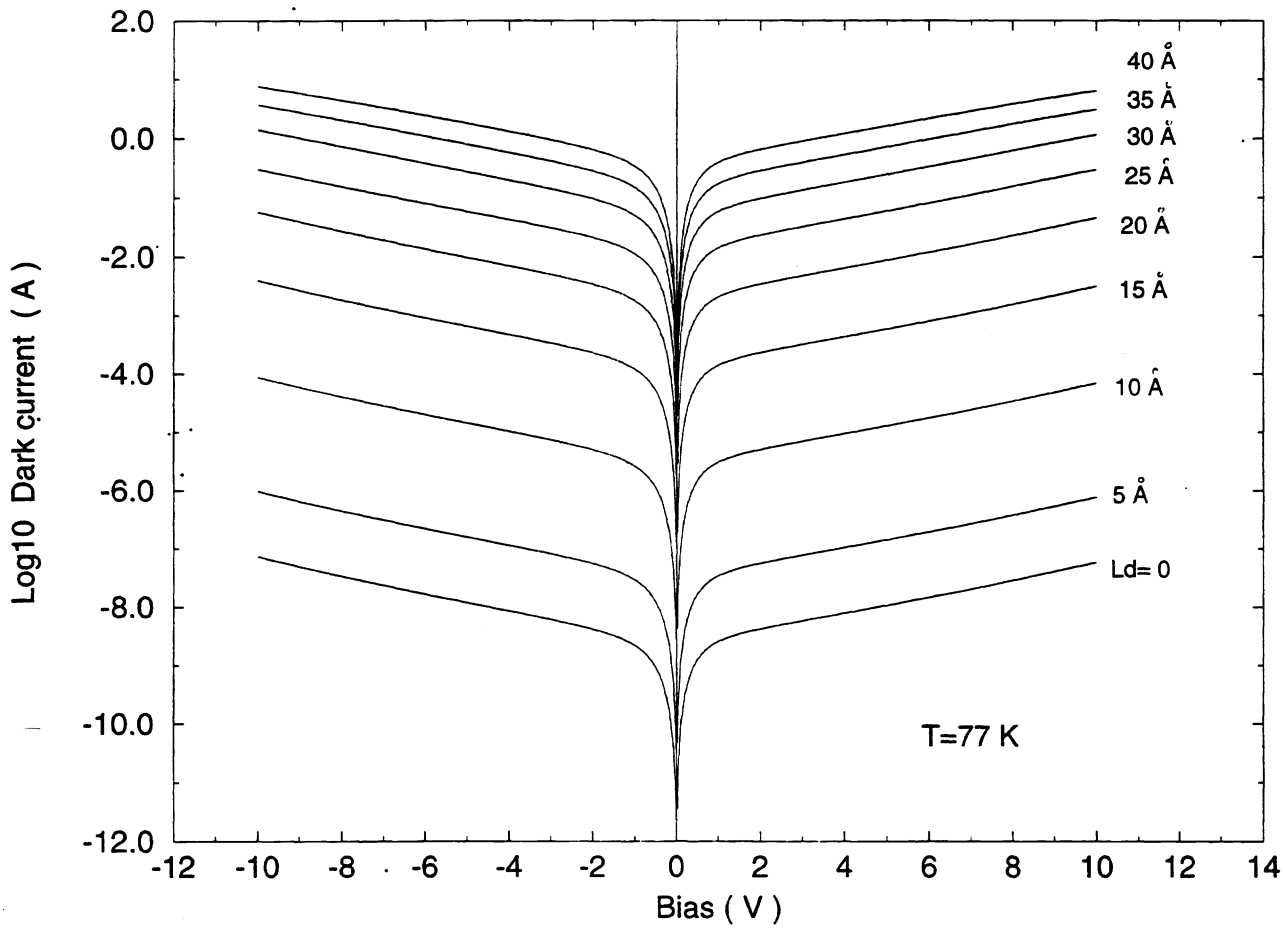

Fig. 6. Dark current vs bias of sample at T= 77 K for L_d=0~40 Å.